KEEPING IT CONSISTENT: ASSESSING MEASUREMENT REPRODUCIBILITY OF A NOVEL ANISOTROPIC PHANTOM FOR HIGHER ORDER DIFFUSION TENSOR MRI SEQUENCES

BY: LAUREN STEPHENS

St. Joseph's Healthcare Hamilton IRC IMAGING RESEARCH CENTRE

Supervisor: Dr. Michael D. Noseworthy
Committee: Dr. Rowley and Dr. Reilly

MASc. Thesis Defense
05/26/25

McMaster University

INTRODUCTION

- Diffusion magnetic resonance imaging (dMRI) measures the diffusion of water molecules in biological tissues
- dMRI is highly susceptible to issues with standardization and reproducibility
  - Crossing-fibre problem
    - 33-90% of white matter voxels contain multiple fibre populations
- There is a need for a robust quality assurance (QA) tool made specifically for diffusion data

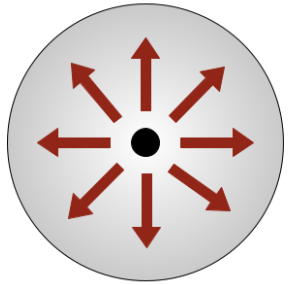

Isotropic diffusion

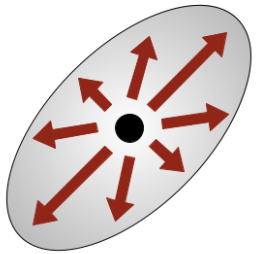

Anisotropic diffusion

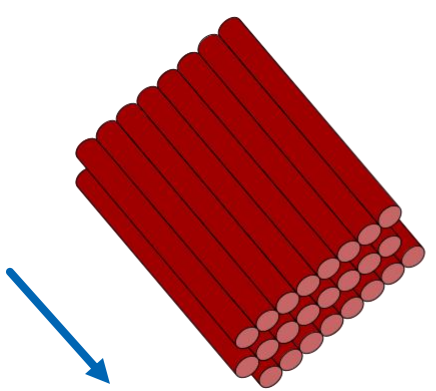

Linear coherent fibres

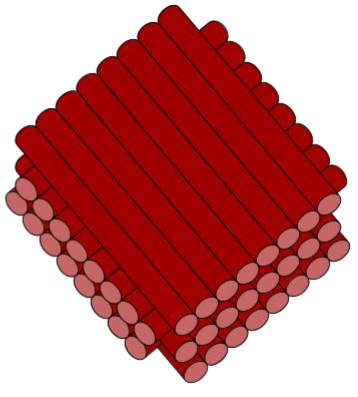

Crossing fibres

INTRODUCTION

- PreOperative Performance (Toronto, ON) have developed a novel anisotropic phantom for QA of diffusion data
  - Mimics the structure of white matter
  - Includes anisotropic fibre bundles with complex crossing and branching structures
- Previous work has been done to validate the phantom for rank-2 tensor metrics across multiple scanner vendors [3]

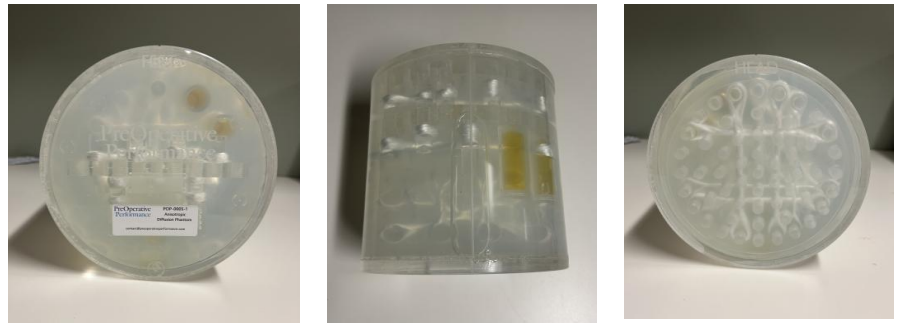

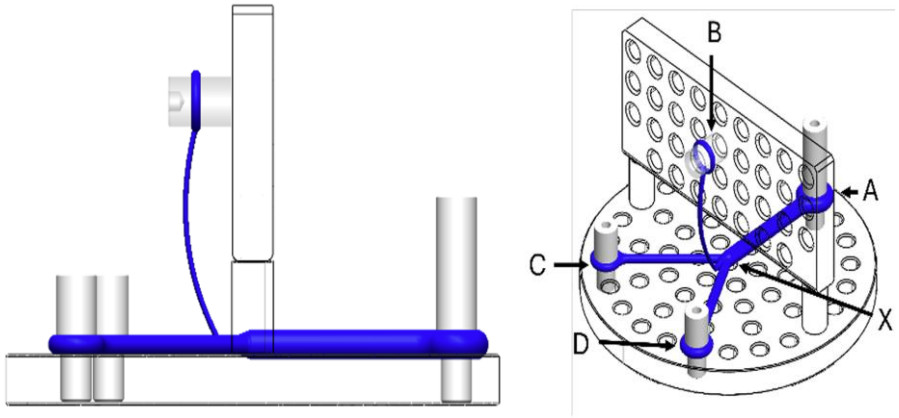

BACKGROUND

- **Diffusion Tensor Imaging (DTI)**
  - Rank-2 tensor representation
  - Assumes Gaussian distribution and single fibre direction
- Diffusion Kurtosis Imaging (DKI)
  - Rank-4 tensor representation
  - Assumes non-Gaussian distribution
- Constrained Spherical Deconvolution (CSD)
  - Spherical convolution with a single-fibre response function
  - Allows multiple fibre directions

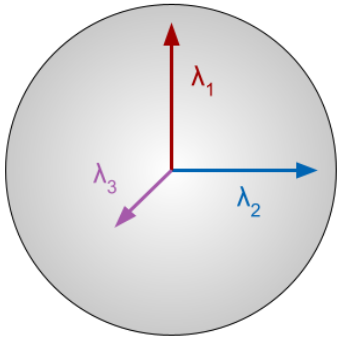

Isotropic diffusion

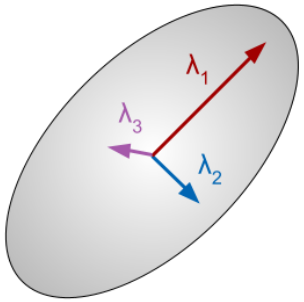

Anisotropic diffusion

McMaster University

BACKGROUND

- Diffusion Tensor Imaging (DTI)
  - Rank-2 tensor representation
  - Assumes Gaussian distribution and single fibre direction
- **Diffusion Kurtosis Imaging (DKI)**
  - Rank-4 tensor representation
  - Assumes non-Gaussian distribution
- Constrained Spherical Deconvolution (CSD)
  - Spherical convolution with a single-fibre response function
  - Allows multiple fibre directions

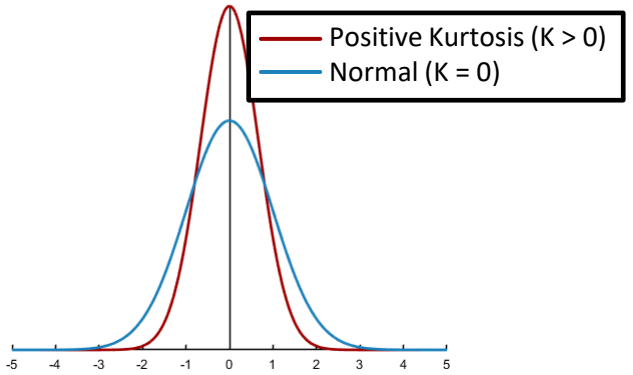

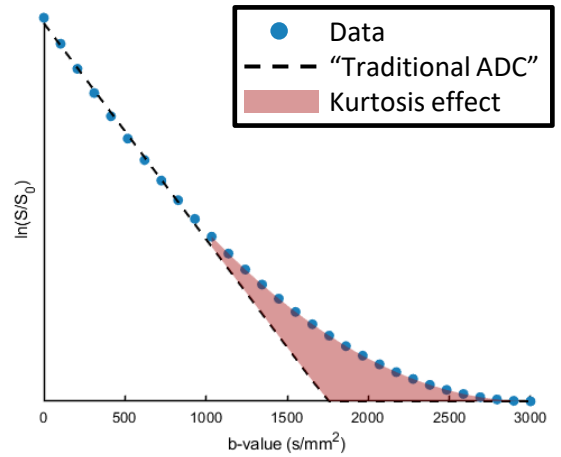

McMaster University

BACKGROUND

- Diffusion Tensor Imaging (DTI)
  - Rank-2 tensor representation
  - Assumes Gaussian distribution and single fibre direction
- Diffusion Kurtosis Imaging (DKI)
  - Rank-4 tensor representation
  - Assumes non-Gaussian distribution
- **Constrained Spherical Deconvolution (CSD)**
  - Spherical convolution with a single-fibre response function
  - Allows multiple fibre directions

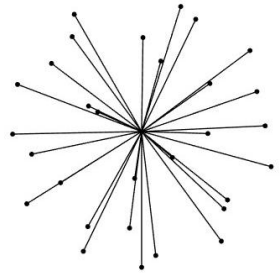

Traditional DTI imaging

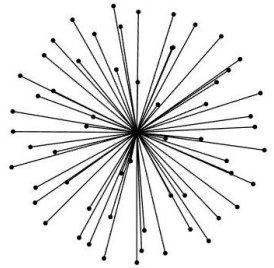

High Angular Resolution Diffusion Imaging (HARDI)

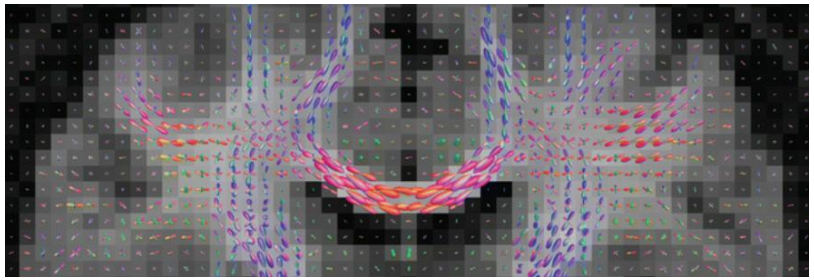

McMaster University

METHODS

- Phantom was imaged across 11 independent trials, with complete removal and repositioning between each scan
  - 30 direction DTI scan
  - 60 direction HARDI scan
  - 90 direction HARDI scan
  - 30 direction DKI scan
- DiPy Python library was used to model the data and generate scalar metric maps
- Metric maps were coregistered and voxelwise data was extracted from 6 ROIs with a variety of fibre geometry
- Mean, standard deviation (SD), coefficient of variation (CoV) and intraclass correlation coefficient (ICC) were calculated from the ROI data

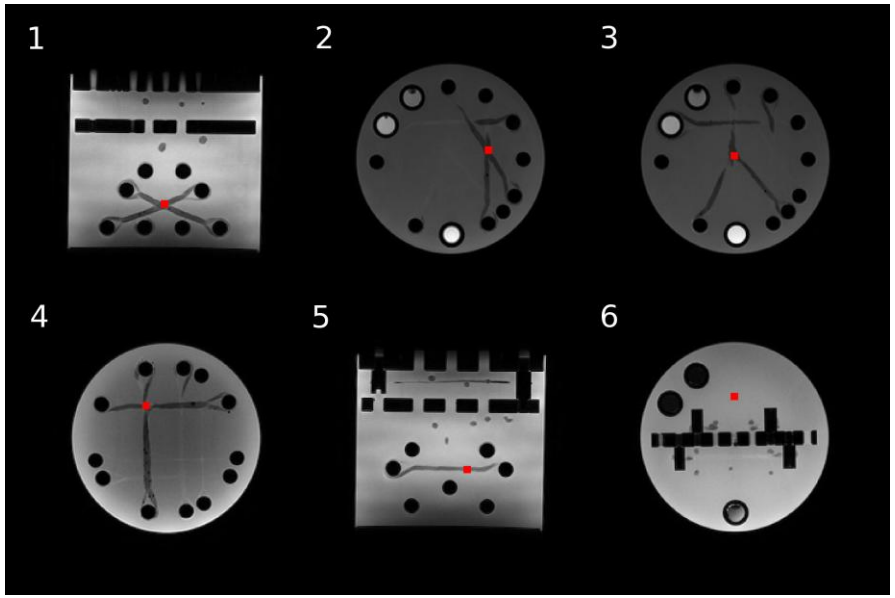

RESULTS: DTI

	DTI		HARDI-60		HARDI-90	
	CoV(%)	ICC	CoV(%)	ICC	CoV(%)	ICC
FA	9.23	0.9155	8.92	0.9335	8.08	0.9415
MD	2.14	0.9315	2.02	0.9417	2.03	0.9380
AD	1.66	0.8321	1.52	0.8846	1.60	0.8957
RD	2.54	0.9418	2.56	0.9469	2.64	0.9424

- Overall, high reproducibility (CoVs < 10%, ICC around 0.9)
- Trend shows CoV decreased and ICC increased when using HARDI acquisitions, showing advantages to using more gradient directions

RESULTS: DTI

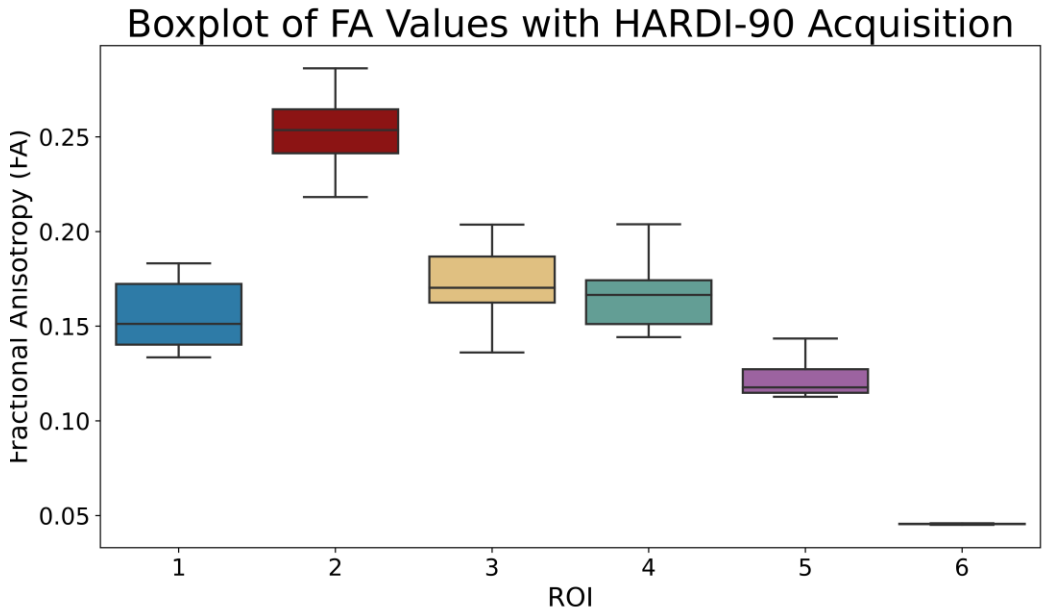

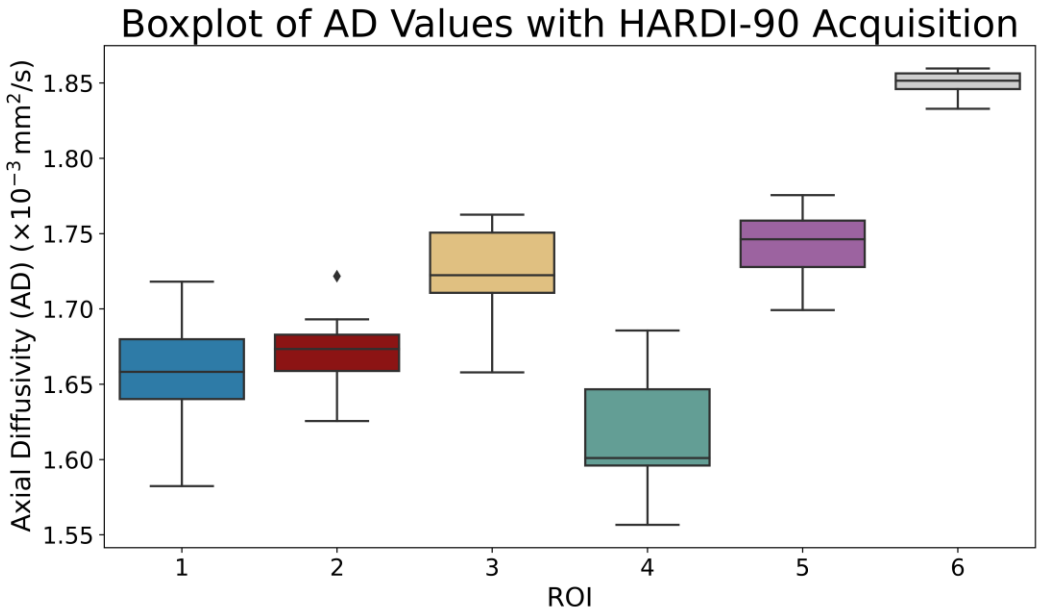

- ROI 2 has the highest FA → could be a result of narrow 30˚ intersection
- ROI 4 has the lowest AD → could be 45˚ intersection causing supressed diffusion along the principal axis
- ROI 5 has the smallest CoV → simple linear fibre aligns well with model assumptions

McMaster University

RESULTS: DKI

	DKI	
	CoV(%)	ICC
KFA	7.36	0.9361
MK	14.99	0.8358
AK	14.04	0.9211
RK	18.62	0.8348

- Higher variability across DKI metrics, especially MK, AK, and RK
- KFA remained stable, with CoV <10% and strong ICC
- Despite higher CoV, ICC values suggest good scan-to-scan repeatability

RESULTS: DKI

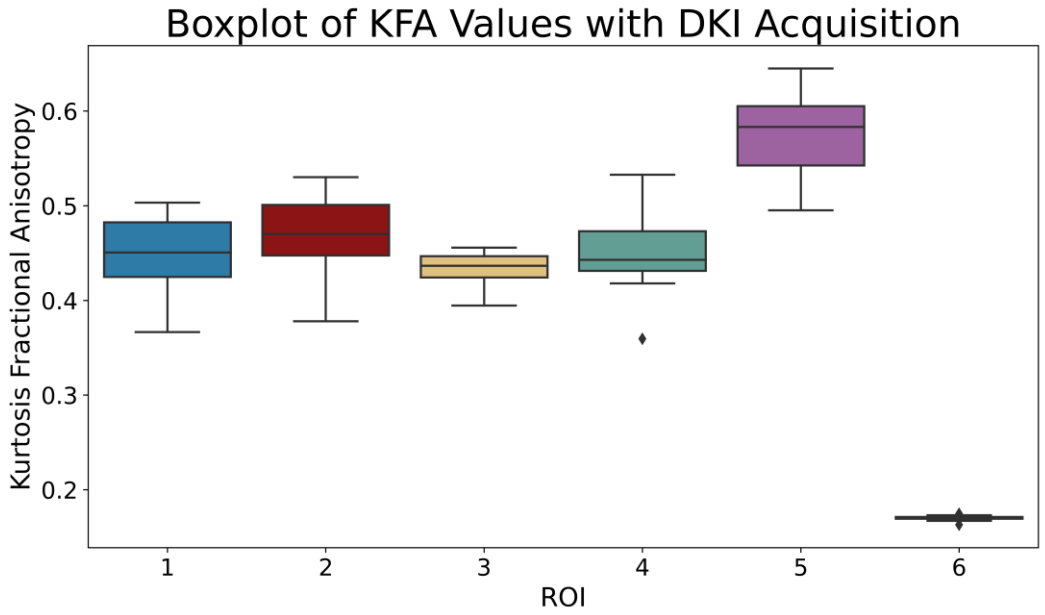

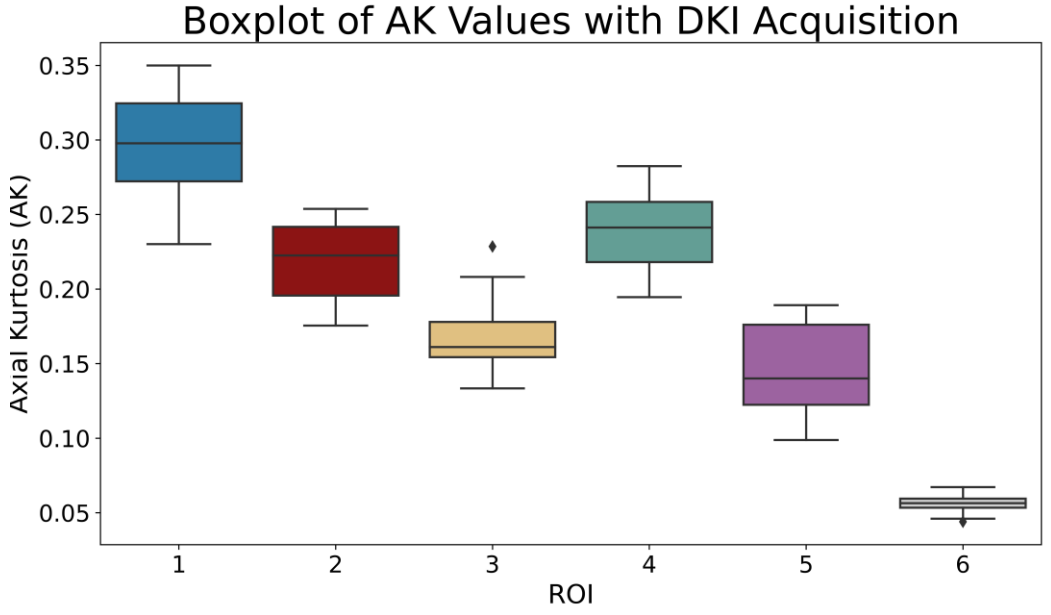

- Unexpectedly, the simple linear geometry (ROI 5) had the highest CoVs
- Very low kurtosis in the isotropic region, indicating that a Gaussian distribution assumption holds well
- No obvious trends with fibre geometry and kurtosis metrics, meaning the relationship between fibre structure and kurtosis is more nuanced

McMaster University

RESULTS: CSD

	DTI		HARDI-60		HARDI-90	
	CoV(%)	ICC	CoV(%)	ICC	CoV(%)	ICC
GFA	6.69	0.6603	4.39	0.8046	4.95	0.8507

- GFA reproducibility improved with higher angular resolution
  - ICC increased from 0.66 to 0.85
- CoV stayed relatively low across protocols

RESULTS: CSD

ROI 1

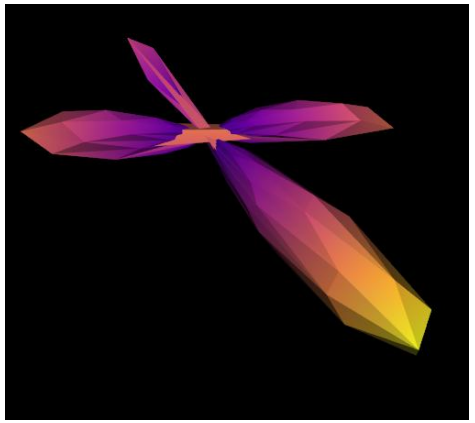

ROI 2

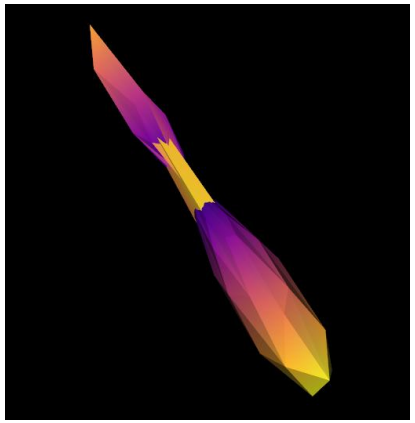

ROI 3

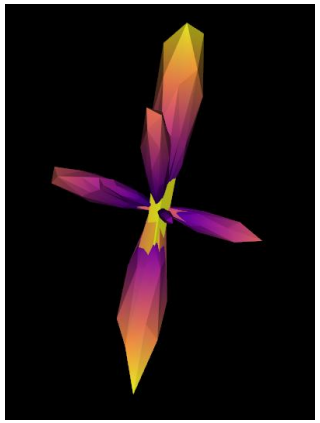

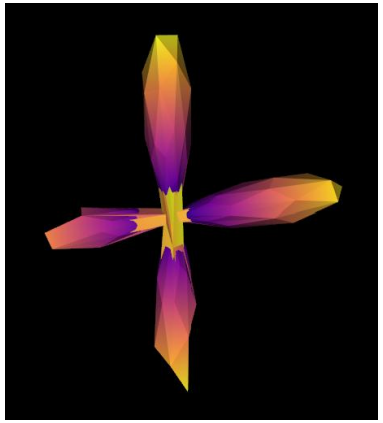

ROI 4

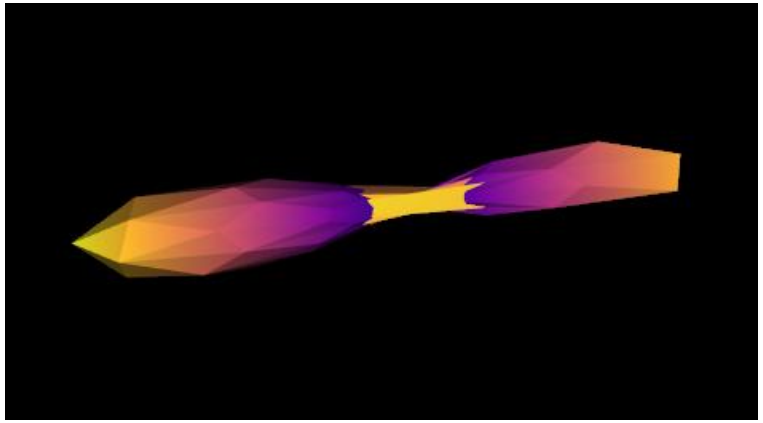

ROI 5

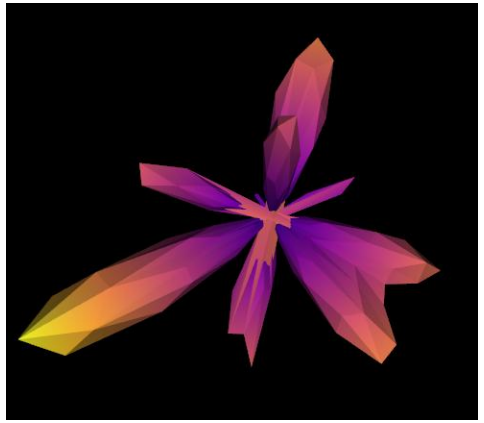

ROI 6

DISCUSSION

- These results highlight that model reproducibility and scalar metric variance is fundamentally linked to fibre geometry
  - Future repeatability studies should aim to include complex fibre geometry in their analysis
- Diffusion kurtosis metrics suffer from high variability
  - This may be due to high b-value acquisitions involving more signal loss and lower SNR
- CSD is able to differentiate crossing and branching fibres in the phantom
  - 30˚ fibre not resolved → could potentially increase number of gradient directions, b-value, or increase l_{max}
- PreOperative Performance phantom is a reliable and effective tool for both traditional DTI and higher order diffusion tensor MRI sequences

St. Joseph's Healthcare Hamilton

IRC IMAGING RESEARCH CENTRE

PreOperative Performance

Thank you!

McMaster University

McMaster School of BIOMEDICAL ENGINEERING

DWI

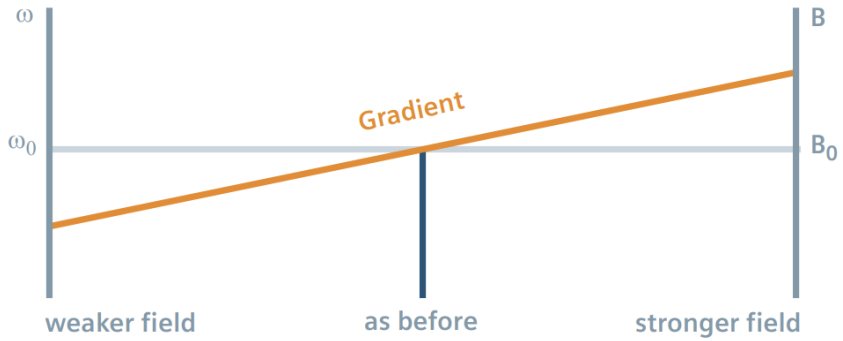

$$\langle r^2 \rangle = 2NDt$$

$$S_b = S_0 e^{-b \cdot D}$$

$$b = \gamma^2 G^2 \delta^2 (\Delta - \frac{\delta}{3})$$

$$ADC = \frac{D_{xx} + D_{yy} + D_{zz}}{3}$$

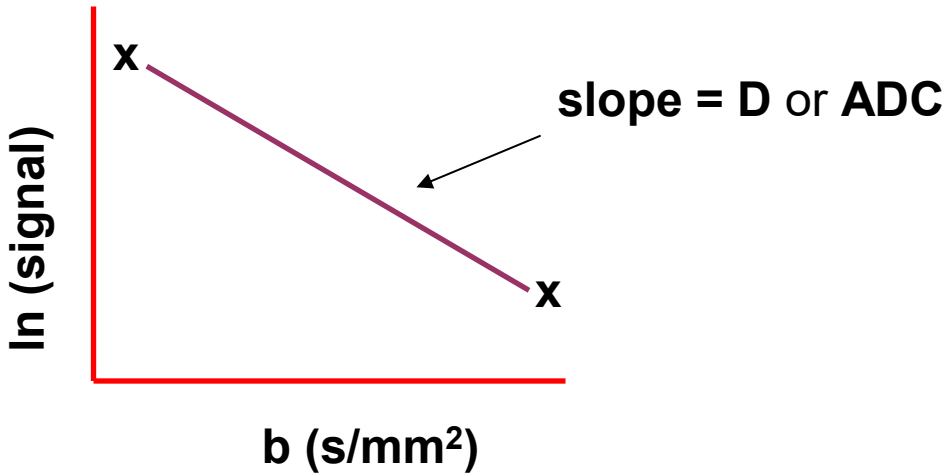

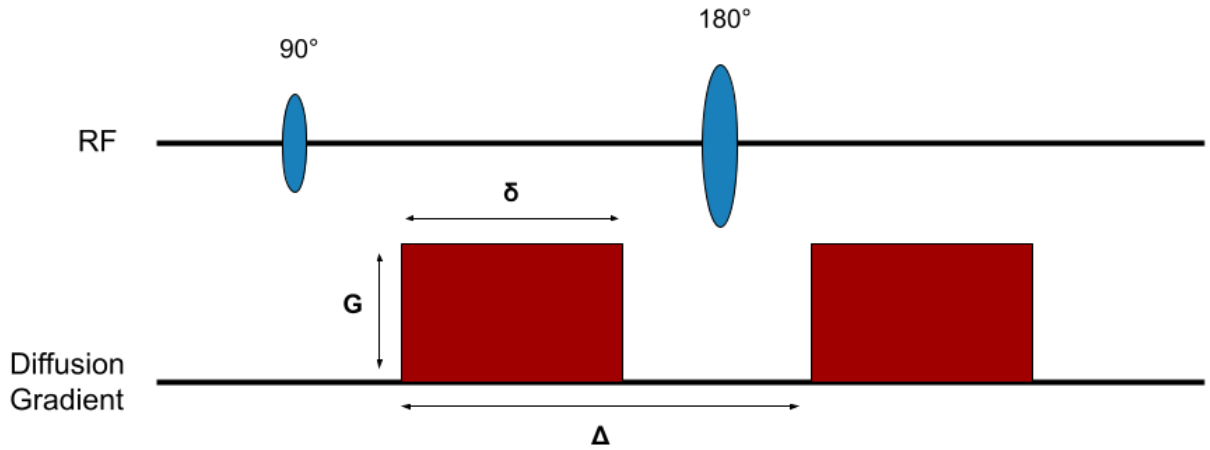

McMaster University

DTI

$$\mathbf{D} = \begin{bmatrix} D_{xx} & D_{xy} & D_{xz} \\ D_{xy} & D_{yy} & D_{yz} \\ D_{xz} & D_{yz} & D_{zz} \end{bmatrix}$$

$$Y = -b\mathbf{X}\boldsymbol{\beta}$$

$$FA = \sqrt{\frac{3}{2}} \cdot \frac{\sqrt{(\lambda_1 - \bar{\lambda})^2 + (\lambda_2 - \bar{\lambda})^2 + (\lambda_3 - \bar{\lambda})^2}}{\sqrt{\lambda_1^2 + \lambda_2^2 + \lambda_3^2}}$$

$$MD = \frac{1}{3}(\lambda_1 + \lambda_2 + \lambda_3)$$

$$Y = \ln\left(\frac{S(b, \mathbf{g})}{S_0}\right)$$

$$AD = \lambda_1 \qquad RD = \frac{1}{2}(\lambda_2 + \lambda_3)$$

$$\mathbf{X} = [g_x^2, g_y^2, g_z^2, 2g_x g_y, 2g_x g_z, 2g_y g_z]$$

$$\boldsymbol{\beta} = [D_{xx}, D_{yy}, D_{zz}, D_{xy}, D_{xz}, D_{yz}]^\intercal$$

$$\mathbf{D} = \mathbf{E}\boldsymbol{\Lambda}\mathbf{E}^\intercal$$

$$\boldsymbol{\Lambda} = \begin{bmatrix} \lambda_1 & 0 & 0 \\ 0 & \lambda_2 & 0 \\ 0 & 0 & \lambda_3 \end{bmatrix} \qquad \mathbf{E} = \begin{bmatrix} \varepsilon_{1x} & \varepsilon_{2x} & \varepsilon_{3x} \\ \varepsilon_{1y} & \varepsilon_{2y} & \varepsilon_{3y} \\ \varepsilon_{1z} & \varepsilon_{2z} & \varepsilon_{3z} \end{bmatrix}$$

$$S(b, \mathbf{g}) = S_0 e^{-b\mathbf{g}^\intercal \mathbf{D} \mathbf{g}}$$

DKI

$$\mathbf{W} = [W_{ijkl}], \quad i,j,k,l \in \{x,y,z\}$$

$$W_{i,j,k,l} = W_{j,i,k,l} = W_{i,j,l,k}$$

$$W_{i,j,k,l} = W_{k,l,i,j}$$

$$K(\mathbf{g}) = \frac{MD^2}{D(\mathbf{g})^2} \sum_{i,j,k,l=1}^{3} g_i g_j g_k g_l W_{ijkl}$$

$$D(\mathbf{g}) = \sum_{i,j=1}^{3} g_i g_j D_{ij}$$

$$\ln\left(\frac{S(b,\mathbf{g})}{S_0}\right) = -bD(\mathbf{g}) + \frac{1}{6}b^2 D^2(\mathbf{g}) K(\mathbf{g})$$

$$KFA = \frac{||\mathbf{W} - \bar{W}\mathbf{I}^{(4)}||_F}{||W||_F}$$

$$MK = \frac{1}{4\pi}\int_{S^2} K(\mathbf{g}) d\mathbf{g}$$

$$AK = K(\mathbf{e}_1)$$

$$RK = \frac{1}{2}[K(\mathbf{e}_2) + K(\mathbf{e}_3)]$$

CSD

$$S(\theta,\phi) = F(\theta,\phi) \otimes R(\theta)$$

$$N = \sum_{l=0,2,4,\ldots}^{l_{max}} (2l+1)$$

$$F(\theta,\phi) \geq 0 \quad \forall\ \theta,\phi$$

$$F(\theta,\phi) = \sum_{l=0,2,4,\ldots}^{l_{max}} \sum_{m=-l}^{l} f_{lm} Y_l^m(\theta,\phi)$$

$$F(\mathbf{f}) = \|\mathbf{Xf} - \mathbf{S}\|^2 + \lambda\|\mathbf{f}\|^2$$

$l_{\max}$	N_{coeffs}
2	5
4	15
6	28
8	45
10	66
12	91

$$(\mathbf{X}^T\mathbf{X} + \lambda\mathbf{B}_{\text{neg}}^T\mathbf{B}_{\text{neg}})\mathbf{f} = \mathbf{X}^T\mathbf{S}$$

$$S(\theta,\phi) = \sum_{l=0,2,4,\ldots}^{l_{max}} \sum_{m=-l}^{l} s_{lm} Y_l^m(\theta,\phi)$$

$$\text{GFA} = \frac{\sqrt{N\sum_{i=1}^{N}(F_i - \bar{F})^2}}{\sqrt{(n-1)\sum_{i=1}^{N} F_i^2}}$$

$$R(\theta) = \sum_{l=0,2,4,\ldots}^{l_{max}} r_l Y_l^0(\theta)$$

$$\mathbf{s}_l = \mathbf{R}_l \cdot \mathbf{f}_l$$

McMaster University

CSD

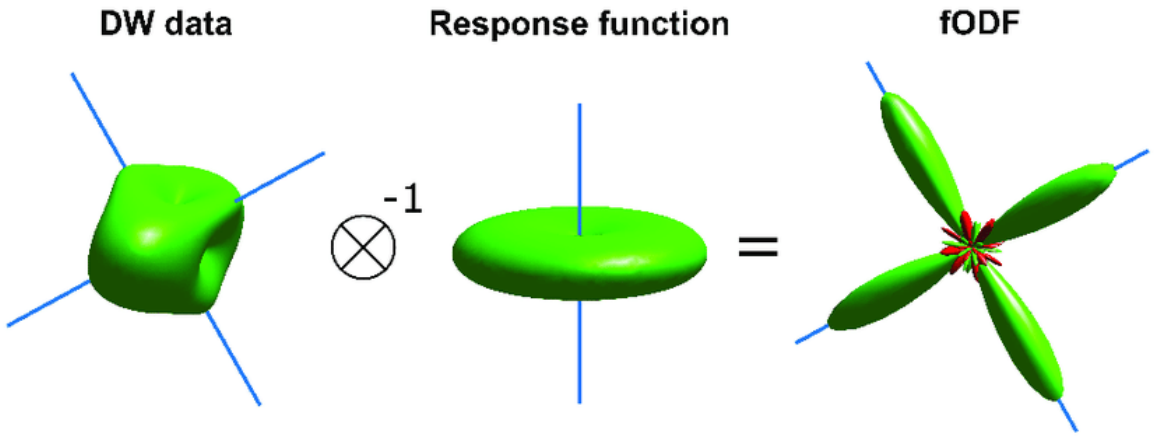
DW data
Response function
fODF
-1
=

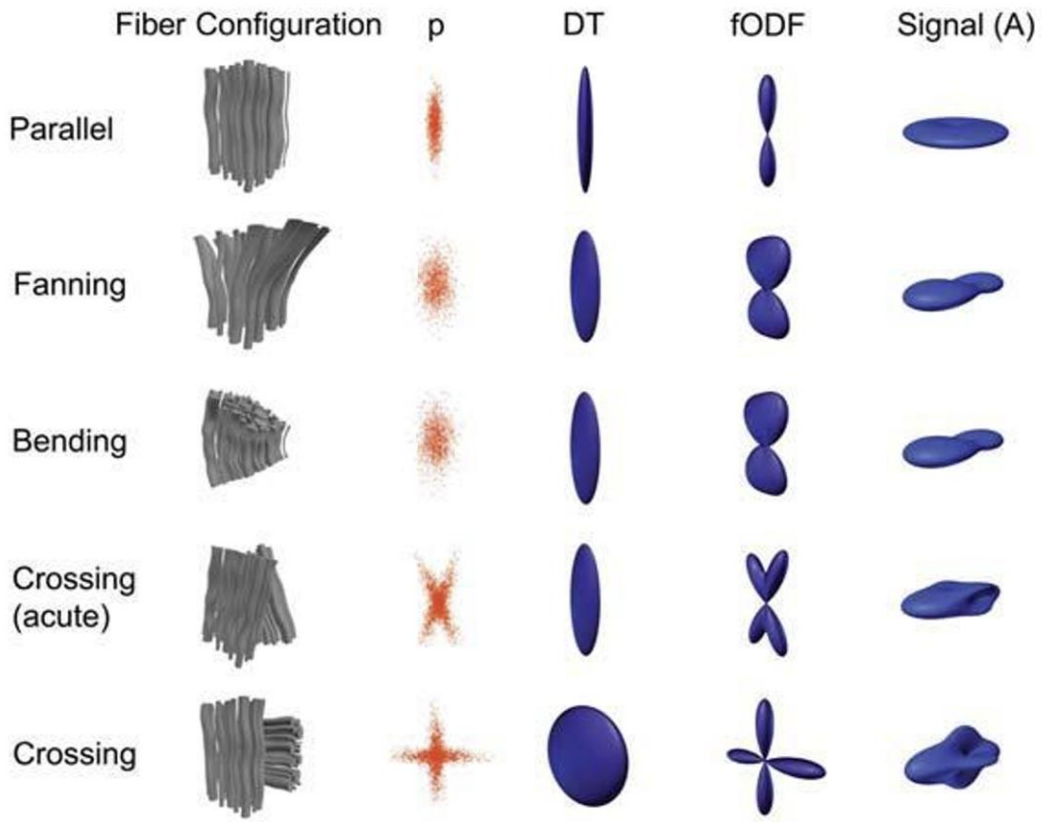
Fiber Configuration
p
DT
fODF
Signal (A)
Parallel
Fanning
Bending
Crossing (acute)
Crossing

SCANNER PARAMETERS

Scan	Directions	B-values	TR/TE (ms)	Flip angle	Voxel size	Slices	Scan Time
T1w FSPGR	—	—	7.94/3.07	12˚	1.0 iso	168	4:37
PROPELLER DWI	3	0, 1000	11000/58.15	110˚	2.5 iso	66	4:57
DTI	30	0, 1000	7000/58.1	90˚	2.5 iso	66	4:05
HARDI-60	60	0, 1300	7000/61.6	90˚	2.5 iso	66	7:35
HARDI-90	90	0, 1300	7000/61.6	90˚	2.5 iso	66	11:05
DKI	30	0, 250-3000	8000/75.1	90˚	2.5 iso	66	32:40

FIGURES FROM THESIS 1

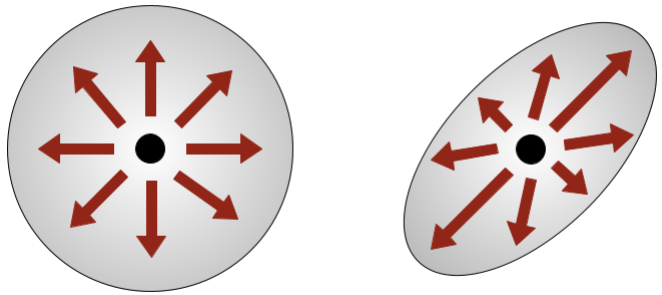

Figure 2.1

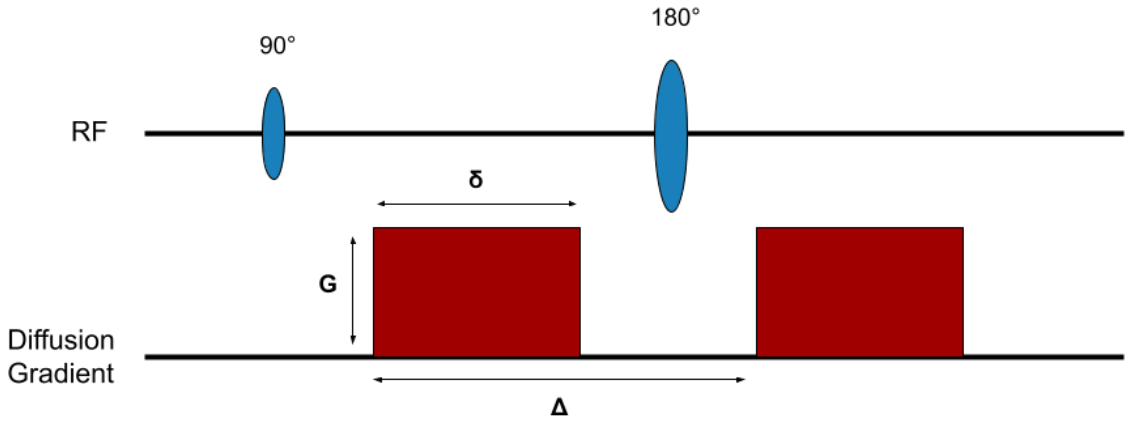

Figure 2.2

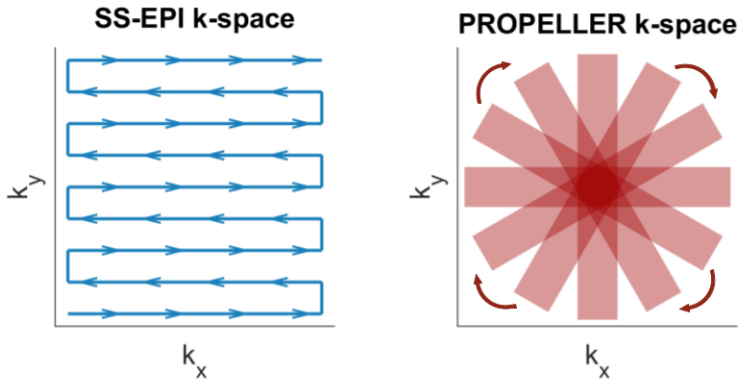

Figure 2.3

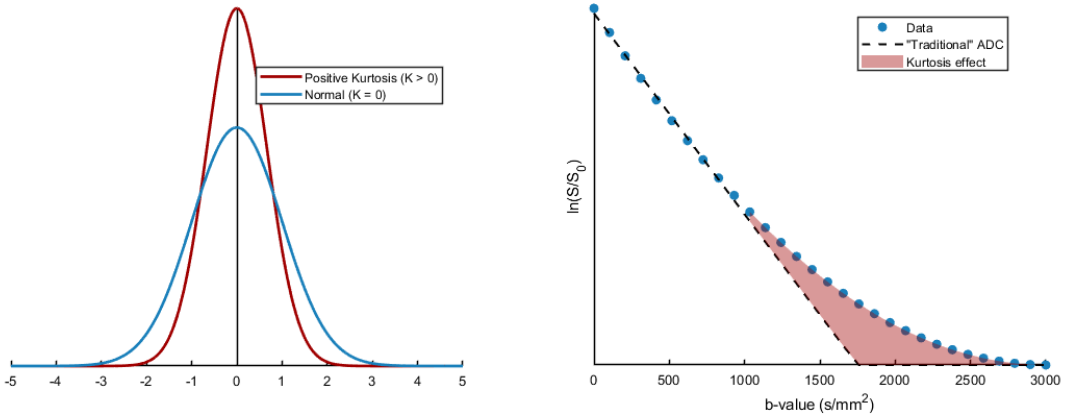

Figure 2.4

McMaster University

FIGURES FROM THESIS 2

$$f_1 S_1(\theta, \phi) + f_2 S_2(\theta, \phi) = S(\theta, \phi) = R(\theta) \otimes F(\theta, \phi)$$

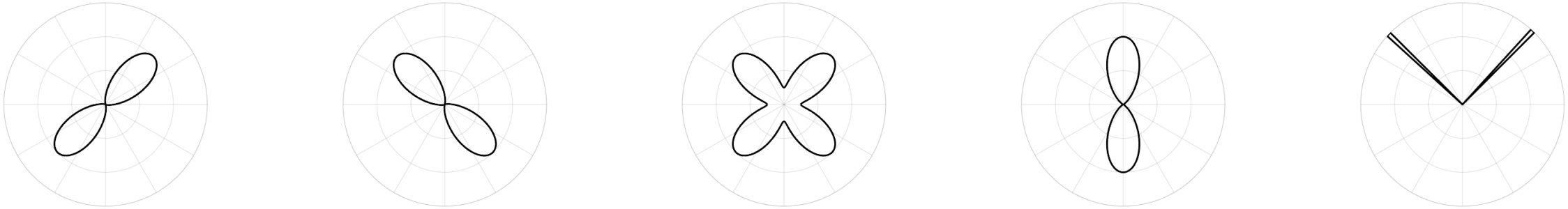

Figure 2.5

Figure 4.1

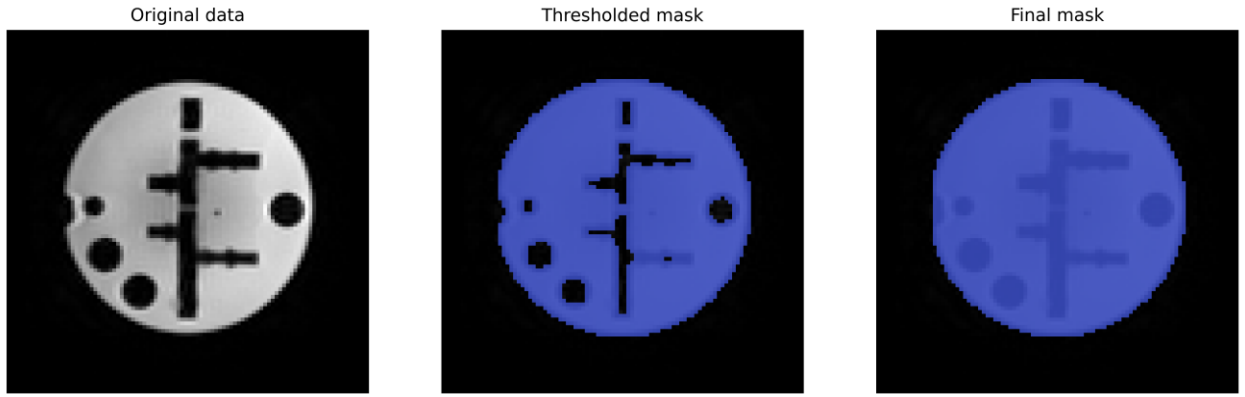

Figure 4.2

FIGURES FROM THESIS 3

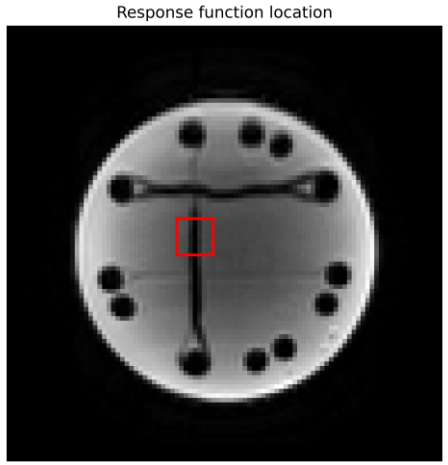

Figure 4.3

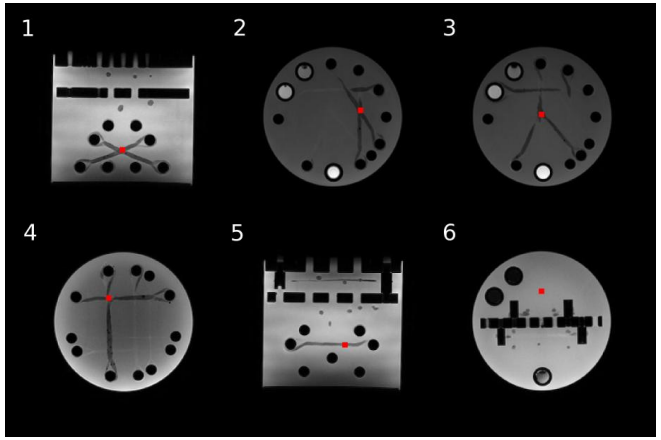

Figure 4.4

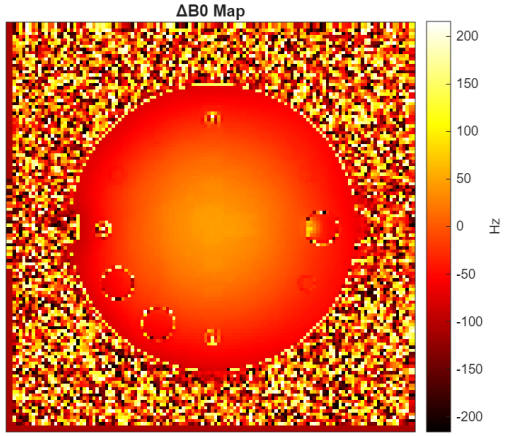

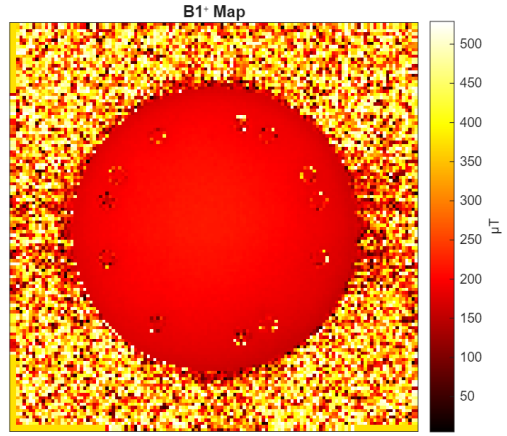

Figure 5.7

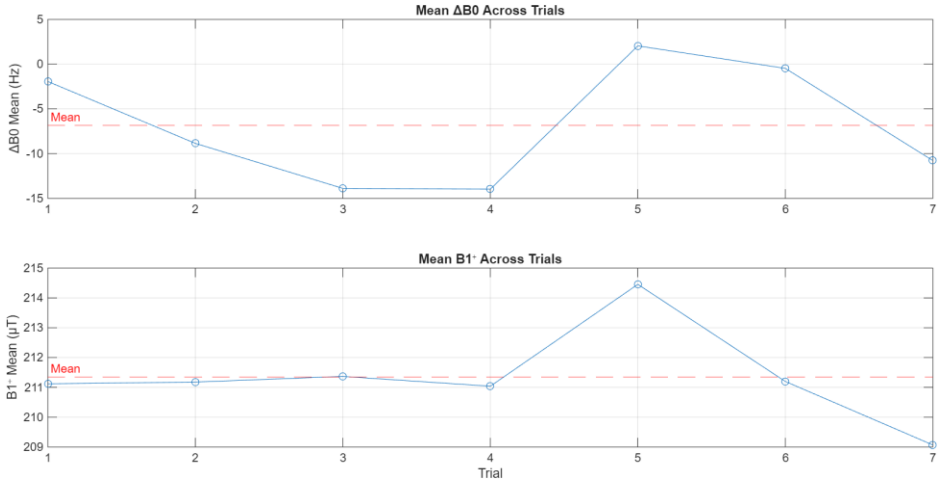

Figure 5.8

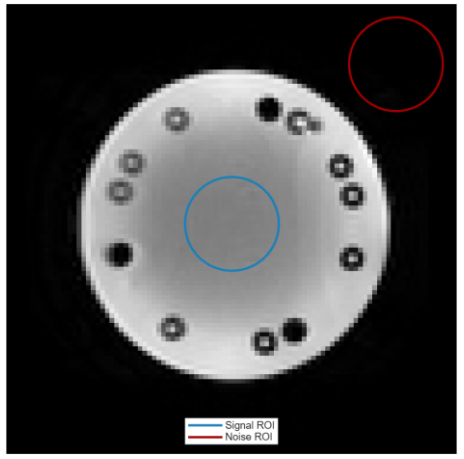

Figure 5.9

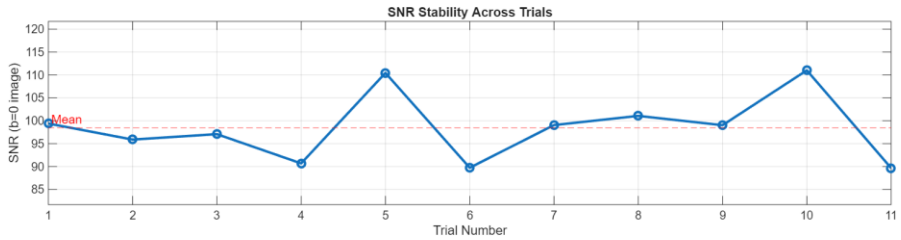

Figure 5.10

McMaster University

FIGURES FROM THESIS 4

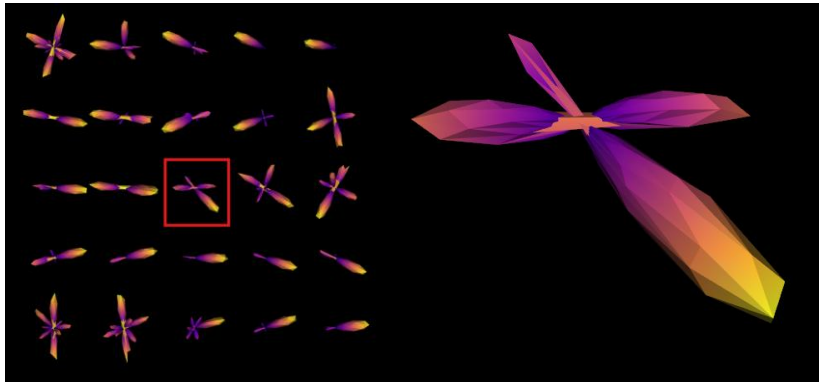

Figure 5.1

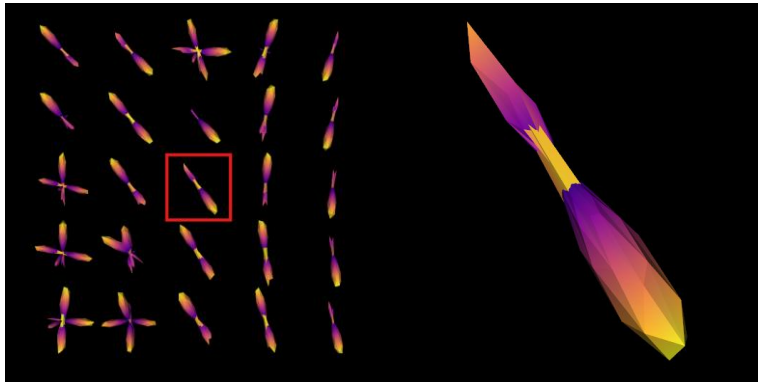

Figure 5.2

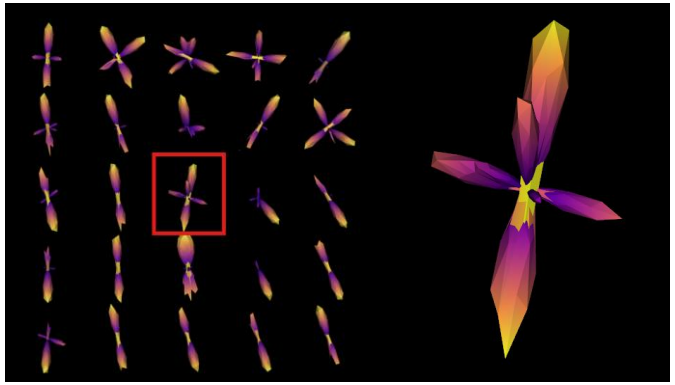

Figure 5.3

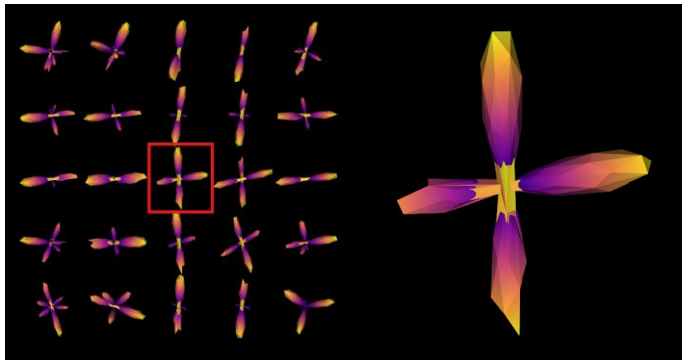

Figure 5.4

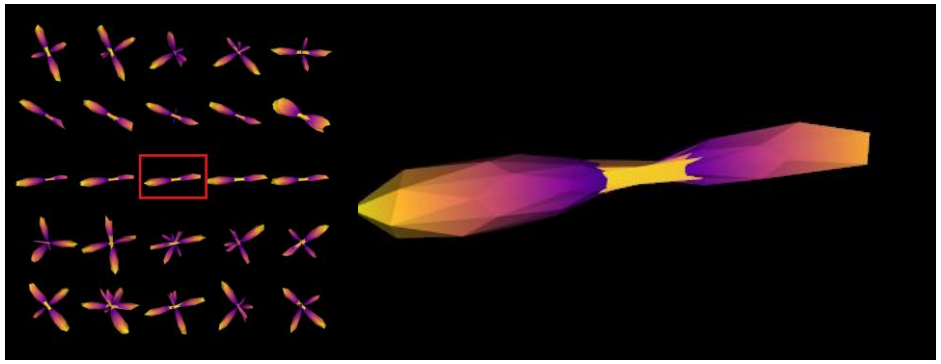

Figure 5.5

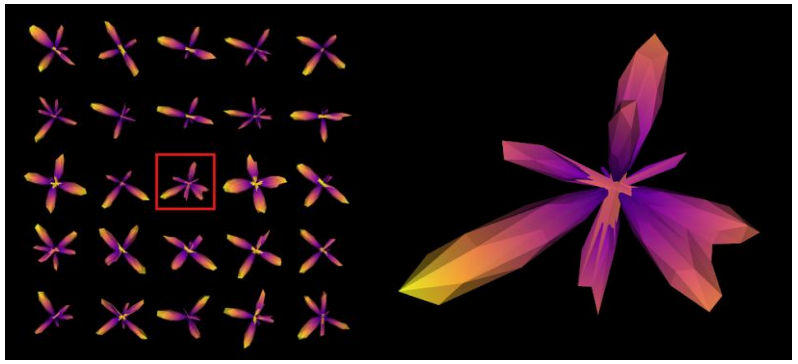

Figure 5.6

FIGURES FROM THESIS 5

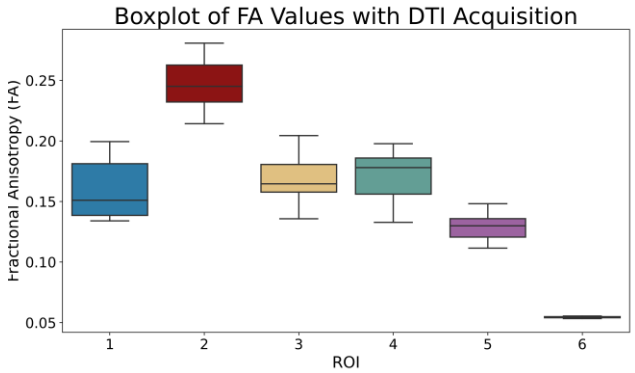

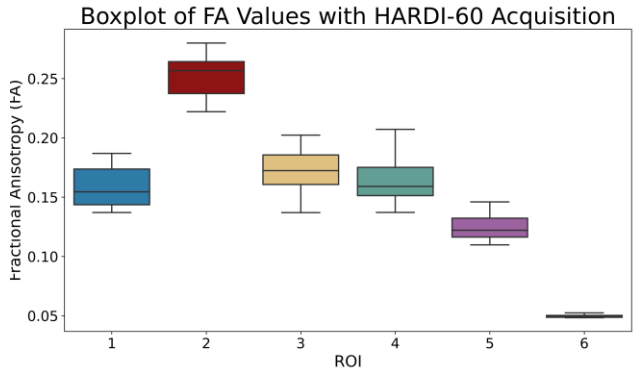

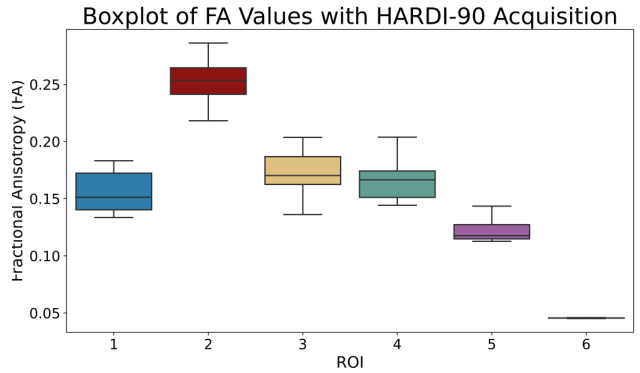

Figure B.1

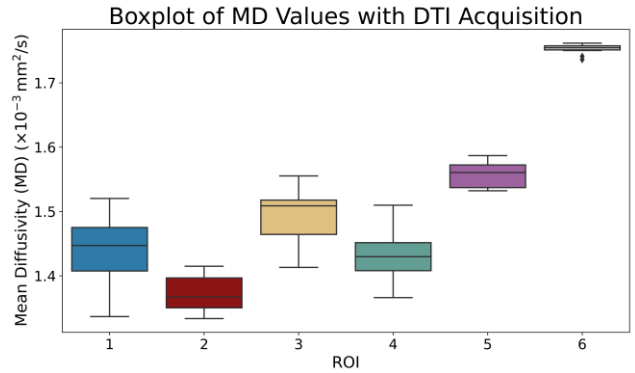

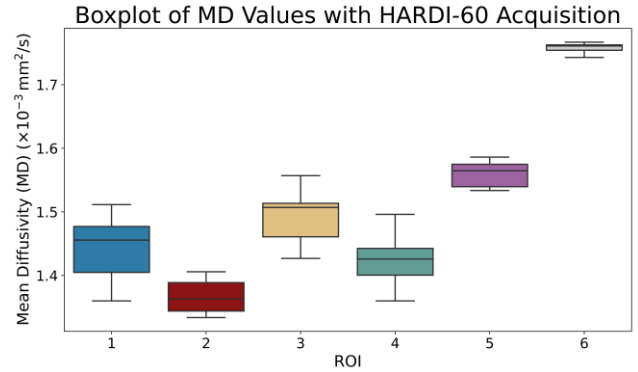

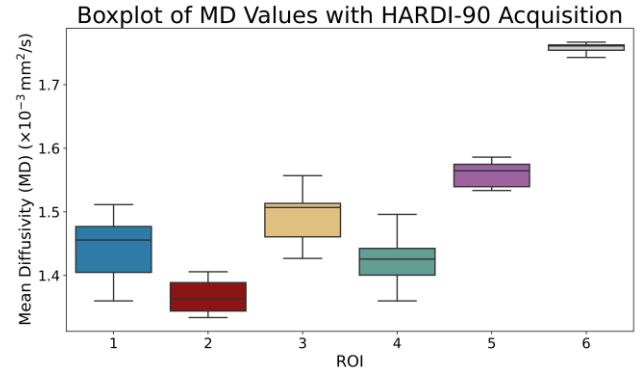

Figure B.2

McMaster University

FIGURES FROM THESIS 6

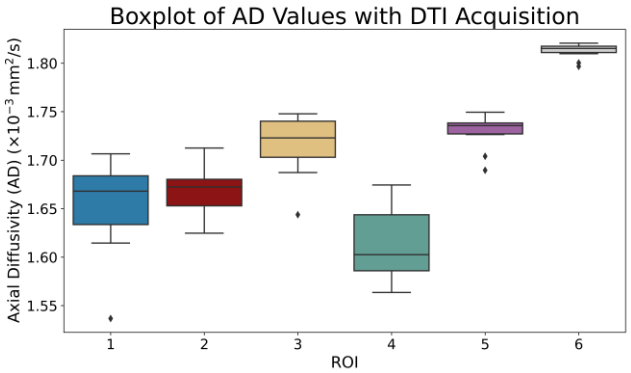

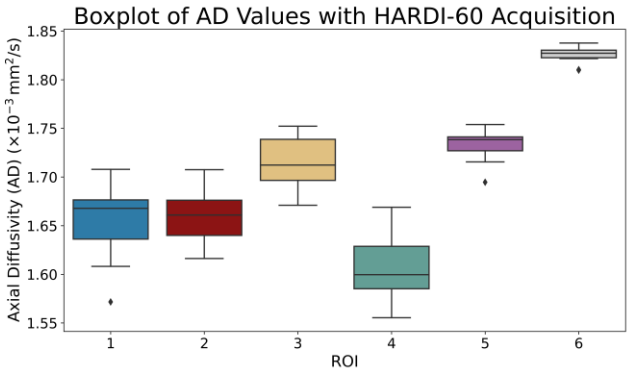

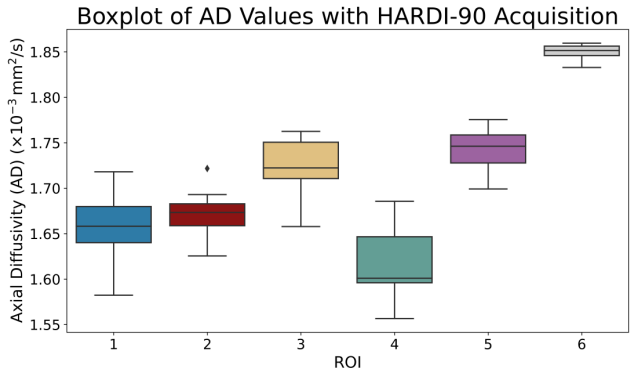

Figure B.3

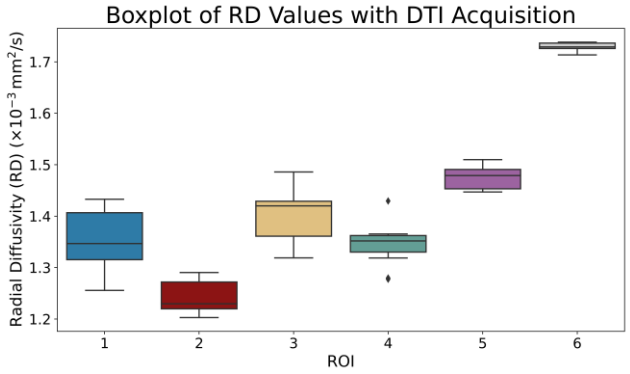

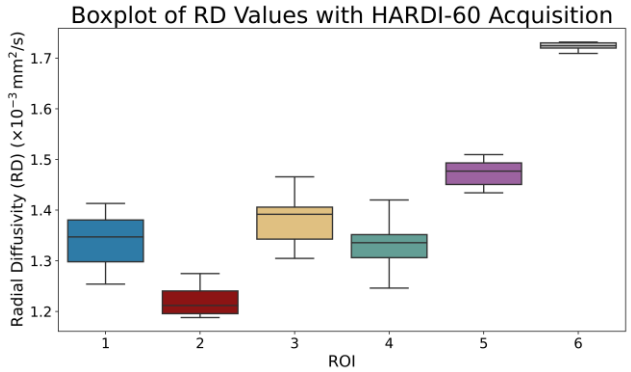

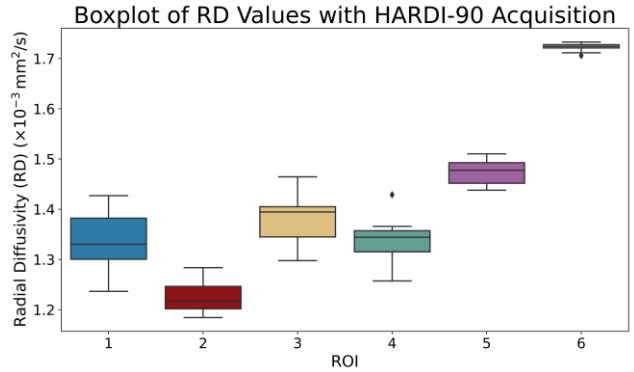

Figure B.4

McMaster University

FIGURES FROM THESIS 7

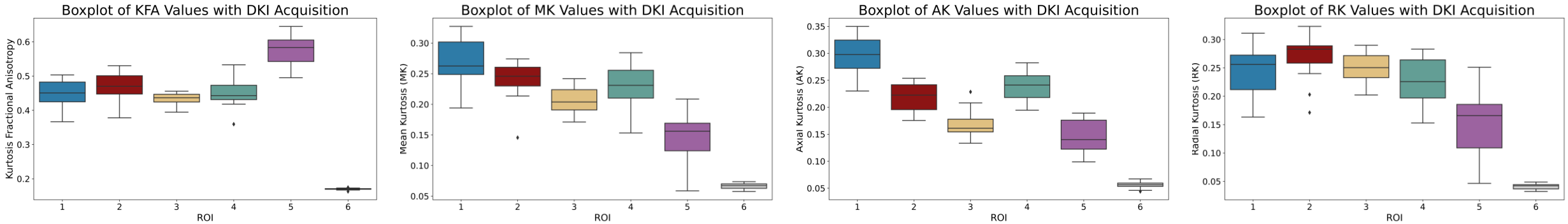

Figure B.5

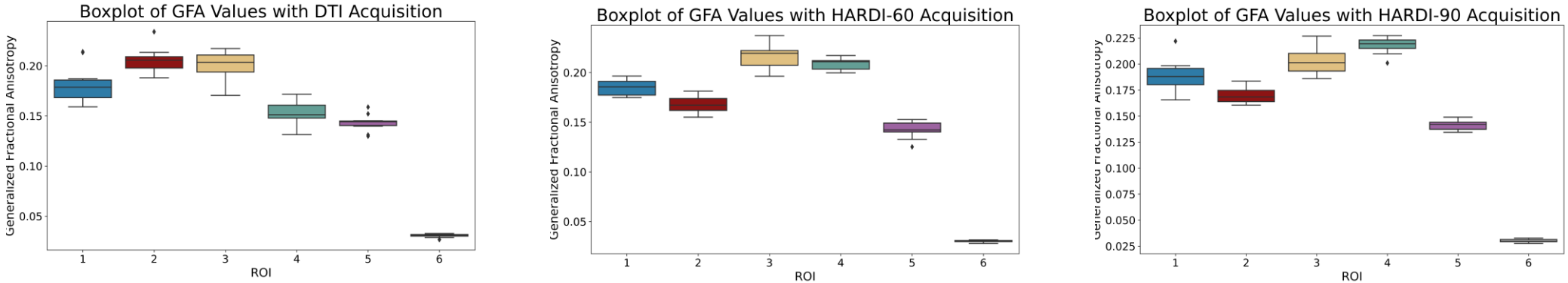

Figure B.6

McMaster University

TABLES FROM THESIS

Table 2.1: Summary of diffusion MRI models with key assumptions, acquisition needs, metrics, and main strengths and limitations.

Model	Assumptions	Requirements	Key Metrics	Strengths and Limitations
DWI	Monoexponential decay	3 directions, single shell	ADC	Simple; lacks directional info
DTI	Gaussian diffusion	$\geq$6 directions, single shell	FA, MD, AD, RD	Captures anisotropy; fails in crossing fibres
DKI	Non-Gaussian diffusion	$\geq$15 dirs, multi-shell	MK, AK, RK, KFA	Models non-Gaussianity; noise-prone
CSD	Multiple fibre populations	$\geq$45 directions, single shell	GFA	Resolves crossings; assumes uniform response

Table 3.1: Anisotropic diffusion phantom repeatability metrics found in the literature

Reference	Phantom	Model(s)	Metric(s)	Metric Values
Teipel et al. (2011) [58]	Polyamide (polyfil) fibres arranged in a ring	DTI	FA	FA CoV: 5.2–9.8%
Hakulinen et al. (2012) [59]	Polyamide (polyfil) fibres arranged in a ring	DTI	FA	FA CoV: 1.3–2.1%
Wilde et al. (2018) [60]	Polymer textile hollow fibres with variable fibre density and tract size	DTI	FA	FA CoV: 4.48–14.88%
Provenzale et al. (2018) [61]	Polypropylene yarn with variable fibre density and tract size	DTI	FA	FA CoV: 2.42–5.59%
de Souza et al. (2019) [62]	Dyneema fishing line with variable filament diameters	DTI	FA, MD	FA CoV: 0.47–4.3% MD CoV: 0.97–3.68%
Kimura et al. (2020) [63]	UHMWPE with variable fibre density bundles	DTI	FA	FA CoV: 1.00–1.89%
Kasa et al. (2020) [64]	3D-printed porous polymer with variable crossing angles (30°–90°)	DTI DKI	MD, AD, RD, MK, AK, RK	MD CoV: ∼1–6% AD CoV: ∼0.75–2.5% RD CoV: ∼1–8.75% MK CoV: ∼0.75–4% AK CoV: ∼1.25–6% RK CoV: ∼0.75–7.75%
Mushtaha et al. (2021) [65]	3D-printed axon-mimetic phantom using GEL-LAY porous filament	DTI DKI	FA, MD, AD, RD, AK, RK, MK	FA CoV: 6.58% MD CoV: 4.88% AD CoV: 2.41% RD CoV: 7.57% MK CoV: 3.62% AK CoV: 15.00% RK CoV: 5.78%

McMaster University